# Prospects for true calorimetry on Kerr black holes in core-collapse supernovae and mergers

Maurice H. P. M. van Putten,[1] Nobuyuki Kanda,[2] Hideyuki Tagoshi,[3] Daisuke Tatsumi,[4] Fujimoto Masa-Katsu,[4] and Massimo Della Valle[5,6]

[1]*Department of Physics, Korea Institute for Advanced Study, 87 Hoegiru, Dongdaemun-Gu, Seoul 130-722, Korea*
[2]*Department of Physics, Graduate School of Science, Osaka City University, Osaka 558-8585, Japan*
[3]*Department of Earth and Space Science, Graduate School of Science, Osaka City University, Osaka 558-8585, Japan*
[4]*National Astronomical Observatory of Japan, 2-21-1 Osawa, Mitaka, Tokyo 181-8588, Japan*
[5]*Istituto Nazionale di Astrofisica—Osservatorio Astronomico di Capodimonte, Salita Moiariello 16, I-80131 Napoli, Italy*
[6]*International Center for Relativistic Astrophysics, Piazzale della Repubblica 2, I-65122, Pescara, Italy*
(Received 28 November 2010; published 24 February 2011)

Observational evidence for black hole spin down has been found in the normalized light curves of long gamma-ray bursts in the BATSE catalog. Over the duration $T_{90}$ of the burst, matter swept up by the central black hole is susceptible to nonaxisymmetries, producing gravitational radiation with a negative chirp. A time-sliced matched filtering method is introduced to capture phase coherence on intermediate time scales, $\tau$, here tested by the injection of templates into experimental strain noise, $h_n(t)$. For TAMA 300, $h_n(f) \simeq 10^{-21}$ Hz$^{-1/2}$ at $f = 1$ kHz gives a sensitivity distance for a reasonably accurate extraction of the trajectory in the time-frequency domain of about $D \simeq 0.07$–$0.10$ Mpc for the spin down of black holes of mass $M = 10$–$12M_\odot$ with $\tau = 1$ s. Extrapolation to advanced detectors implies $D \simeq 35$–$50$ Mpc for $h_n(f) \simeq 2 \times 10^{-24}$ Hz$^{-1/2}$ around 1 kHz, which will open a new window to rigorous calorimetry on Kerr black holes.

DOI: 10.1103/PhysRevD.83.044046 PACS numbers: 04.30.Db

## I. INTRODUCTION

Calorimetry and spectroscopy on all radiation channels will be key to identifying Kerr black holes in the Universe [1]. They may be central to some of the core-collapse supernovae (CC-SNe, [2]) and mergers of neutron stars with another neutron star or with a companion black hole ([3])—the currently favored astronomical progenitors of cosmological gamma-ray bursts (GRBs). While all short GRBs are probably produced by mergers, the converse need not hold, in general. Black holes with a neutron star companion should have a diversity in spin [4]. These mixed binaries can be short- and long-lived, depending on the angular velocity of the black hole. It predicts that some of the short GRBs, produced by slowly spinning black holes, also feature x-ray afterglows [5], as in GRB050509B [6] and GRB050709 [7–9]. Produced by rapidly rotating black holes, long GRBs are expected to form in CC-SNe from short, intraday period binaries ([10,11]), but also from mergers with a companion neutron star [4] or out of the merger of two neutron stars [12,13].

A diversity in the origin of long GRBs in CC-SNe and mergers naturally accounts for events with and without supernovae, notably GRB060614 [14,15]; with and without pronounced x-ray afterglows [16]; and in wind versus constant-density host environments, which are relevant to recent studies of extraordinary Swift and Fermi-LAT events [17,18].

Rapidly rotating black holes can sweep up surrounding matter and induce the formation of multipole mass moments. In this process, spin energy is catalytically converted to a long-duration gravitational-wave burst (GWB, [19,20]). For stellar mass black holes, this output may be detected by advanced gravitational-wave detectors for events in the local Universe. As candidate inner engines to long GRBs, evidence for the associated spin down of the black hole has been found in the normalized light curve of 600 long GRBs in the BATSE catalog [16].

The high-frequency range of the planned advanced detectors LIGO-Virgo [21,22], the Large-scale Cryogenic Gravitational-wave Telescope ([23]) and the Einstein Telescope ([24]) covers the quadrupole emission spectrum of orbital motions around stellar mass black holes, thus establishing a window to rigorously probe the innermost workings of GRBs and some of the CC-SNe.

We anticipate an event rate for long GWBs of 0.4–2 per year within a distance of 100 Mpc from the local event rate of long GRBs [25]. It compares favorably with that of mergers of binary neutron stars (e.g., [26,27]). Since the local event rate of type Ib/c supernovae is $\sim$80 per year within a distance of 100 Mpc, the branching ratio of type Ib/c supernovae into long GRBs is, therefore, rather small, about 0.5 [11] up to $\sim$2.5% [25]. It suggests the existence of many failed GRB supernovae, notably supernovae with relativistic ejecta, supernovae with pronounced aspherical explosions, and radio-loud supernovae (e.g., [28] and references therein). Therefore, the rate of events of interest to potential bursts in gravitational waves appears to be 1–2 orders of magnitude larger than the event rate of successful GRB supernovae. In addition, type II SNe, whose event rates are 3–4 times larger those that of type Ib/c [29,30], may also explode and expand asymmetrically [31,32], suggesting a significant additional potential for gravitational-wave–burst production.

 

A blind rather than a triggered search for burst events in the local Universe seems to be appropriate by taking advantage of the all-sky monitoring capability of the gravitational-wave detectors, in view of a beaming factor of gamma-ray bursts of $f_b < 10$ ($\theta > 25$ deg) up to a few hundred ($\theta \sim 4$ deg, [25,33,34]). A blind search is also expected to be competitive with current X/optical surveys for detecting the shock breakout associated with emerging CC-SNe, as they last only a few dozens of minutes up to a few hours, and it naturally includes the possibility of long GRBs coming from merger events with no supernova, which may be exemplified by the long event GRB060614 of duration 102 s discovered by Swift.

While the energy output in long GWBs produced by rapidly rotating black holes should be large, searching for these bursts by matched filtering is challenging in view of anticipated phase incoherence due to turbulent magneto-hydrodynamical motions in the inner disk or torus.

Here, we focus on the detection of a trajectory in the time-frequency domain produced by long GWBs, satisfying phase coherence on short up to intermediate time scales. This objective goes further than the detection of a burst signal, with the aim to extract reasonably accurate information on the burst evolution. Inevitably, the sensitivity distance for extracting trajectories is considerably more conservative than the sensitivity distance for a detection *per se*.

We shall discuss a new matched filtering detection algorithm to detect trajectories in the time-frequency domain for long GWBs with slowly varying frequencies lasting tens of seconds with intermittent phase coherence. For a burst lasting 50 s, for example, the algorithm searches by matched filtering, using segmented templates on a time scale of, e.g., 1 s. This procedure gives a compromise between optimal matched filtering, applicable to phase coherence extending over the entire burst duration as in the binary coalescence of two black holes, and second-order methods by the correlation of independent detector signals in the time domain. For our example, the compromise results in a sensitivity distance below that of optimal matched filtering by a factor of about $\sqrt{50} \sim 7$ and an improvement by a factor of $\sqrt{1000} \simeq 30$ over second-order methods for signals around 1 kHz.

In Sec. II, we discuss the astronomical origin of long GRBs both from possible CC-SNe and mergers. In Sec. III, we introduce a model and template for long GWBs from rapidly rotating Kerr black holes. In Sec. IV, we describe the proposed time-sliced matched filtering (TSMF) search algorithm and the evaluation of the sensitivity distance for a reasonably accurate extraction of trajectories in the time-frequency domain. Our findings are summarized in Sec. V.

## II. LONG GRBS FROM CC-SNE AND MERGERS

As universal inner engines, rapidly rotating Kerr black holes can explain long GRBs from both CC-SNe and some of the mergers. They enable long GRBs with supernovae exclusively in star-forming regions with stellar wind host environments and without supernovae such as GRB060614, both in and away from star-forming regions, including halos such as GRB070125.

Some recent Swift and Fermi-LAT detections of long GRBs show events with and without x-ray afterglows, such as GRB050911, interstellar medium (ISM)-like constants or windlike $r^{-2}$ density profiles in the local host environments, and a diversity in distances from a local host galaxy, as summarized in Table I. This phenomenology is not accounted for by CC-SNe alone and suggests that some of the long GRBs are associated with mergers, otherwise sharing a common long-lived inner engine.

Radiative processes around Kerr black holes are driven by frame dragging, expressed in terms of a nonzero-angular velocity $\omega$ of zero-angular momentum observers. It gives rise to high-energy emissions along the spin axis by the induced potential energy $E = \Omega J_p$ for particles with angular momentum $J_p$ [16] and, contemporaneously, to a spin connection to surrounding matter by equivalence in topology to pulsar magnetospheres [4]. Thus, observations on high-energy emissions (in gamma rays, afterglow emissions, and, possibly, ultra-high-energy cosmic rays) from

TABLE I. Proposed core-collapse and merger progenitors to a Swift sample of long GRBs.

| GRB | Redshift | Duration(s) | Host | Constraint[a] | Type |
|---|---|---|---|---|---|
| 050820A [37,38] | 1.71 | $13 \pm 2$ | UVOT $< 1$ arcsec | ISM-like [17] | Merger |
| 050904 [39–41] | 6.29 | $225 \pm 10$ | Unseen low star-forming region | Dense molecular cloud [57] | CC-SN |
| 050911 | 0.165 | 16 | Cluster Edinburgh-Durham Galaxy Catalogue 493 | No x-ray afterglow [42] | Merger [58,16] |
| 060418 [43–46] | 1.490 | $(52 \pm 1)$ | ISM spectrum | $\gamma$-ray efficiency [17] | Merger |
| 060505 [47] | 0.09 | 4 | Spiral, ionized atomic hydrogen | No SN [c] | Merger |
| 060614 [47,50][b,c] | 0.13 | 102 | Faint star-forming region | No SN[b,c] | Merger [14,15] |
| 070125 [51–53] | 1.55 | >200 | Halo | ISM-like [53] | Merger |
| 080319B [54–56] | 0.937 | 50 | Faint dwarf galaxy | Wind [17] | CC-SN |

[a]"ISM-like" refers to a constant host density; wind refers to a $r^{-2}$ density profile associated with a massive progenitor [35,36].
[b]Observed with an 8.2 m telescope, [48].
[c]Observed with a 1.5 m telescope, [49].

leptonic jets, as well as on low-energy emissions (in gravitational waves, MeV neutrinos, and magnetic winds, powering a supernova or a radio burst), emanating from matter are required for full calorimetry.

According to the Kerr metric, rotating black holes are energetically very similar to spinning tops in the sense of having a ratio

$$\frac{E_{\rm rot}}{\Omega_H J} = \frac{1}{2}\cos^{-2}(\lambda/4) = 0.5 - 0.5858 \qquad (1)$$

close to the Newtonian value of $\frac{1}{2}$ for all spin rates $\Omega_H$ associated with the angular momentum $J$ and rapidity $\lambda$, where $\sin\lambda = a/M$ and $a = J/M$. In the absence of a small parameter, $E_{\rm rot}$ reaches 29% of the total mass energy of an extreme Kerr black hole, or about $1.6–6 \times 10^{54}$ erg for a black hole in the mass range $4–14 M_\odot$.

Existing calorimetry on GRB afterglows points to true energies in gamma rays $E_\gamma$ and kinetic energies $E_{\rm KE}$ broadly distributed around $1 \times 10^{51}$. These estimates apply to the subsample of GRBs for which achromatic breaks in their light curves have been determined, as the basis for estimating the half-opening angle of the beamed outflow by a model fit for the interaction with the host environment comprising about seven parameters [17]. It has been well-recognized that there is considerable uncertainty in this estimation procedure, also in assuming a uniform luminosity profile across the outflow. Quite generally, the outflow may comprise a baryon-poor ultrarelativistic inner jet and a possibly baryon-rich and mildly relativistic collimating wind (e.g., [20,59–65]), while the inner jet may be structured in different ways, e.g., with the highest luminosity reached at the boundary with the collimating wind [16]. Despite these uncertainties and model assumptions, exceptional events [17] point to $E_\gamma \simeq 2.25 \times 10^{52}$ erg (GRB060418) and $E_{\rm KE} \simeq 3.56 \times 10^{52}$ erg (GRB050820A), well above their typical values around $1 \times 10^{51}$ erg. *And yet*, these energies represent a *minor* fraction of about 1% of $E_{\rm rot}$ or less, following (1).

The common properties in durations, spectra, and true energies in the prompt gamma-ray emissions in long GRBs point to a universal inner engine as the outcome of the apparent diversity in astronomical origin and host environment (Table I), whose lifetime is intrinsic to the physical state of the energy reservoir itself. By the above, identifying it with the rapid spin of the central black hole leaves about 99% of the spin energy unaccounted for and a similar fraction "unseen" in emissions in gravitational waves and MeV neutrinos, the remainder of which may be dissipated in the event horizon.

## III. LONG-DURATION GRAVITATIONAL-WAVE BURSTS FROM KERR BLACK HOLES

The lowest-order, axisymmetric component of magnetic fields in an accretion disk can form a torus magnetosphere around a black hole [19]. In its lowest-energy state [19,66–69], a rapidly spinning black hole can, hereby, establish a spin connection to its surrounding disk or torus for the catalytic conversion of a major fraction of its spin energy into a variety of radiation channels.

Quite generally, the torus magnetosphere will be highly time-variable. When the central black hole spins rapidly, the interaction is governed by the variance of the net poloidal magentic flux of the magnetic field to mediate energy and angular momentum transfer. The black hole, hereby, sweeps up the inner face of the torus to excite nonaxisymmetric instabilities, giving rise to gravitational radiation, MeV neutrinos, and magnetic winds. This state of suspended accretion lasts for the lifetime of the rapid spin of the black hole and sets the duration of a possibly accompanying GRB. During viscous spin down, a major fraction, if not most, of the spin energy is dissipated unseen in the event horizon, creating astronomical amounts of Bekenstein entropy.

Based on the Kerr metric, the model template produced by matter swept up by a central black hole shows negative chirp with late-time asymptotic frequency [14]

$$f_{\rm GW} = 595–704\ {\rm Hz}\left(\frac{10 M_\odot}{M}\right) \qquad (2)$$

as a function of the initial mass $M$ and for a range of initial spin of the black hole. The negative chirp represents the expansion of the inner disk or torus during the spin down of the black hole on a viscous time scale. Thus, the merger of two neutron stars features a late-time frequency of 1.5–2 kHz defined by the sum of the mass of the two progenitor neutron stars ($2 \times 1.5–2 M_\odot$, where the high masses refer to PSR J0751+1807 [70] and PSR J1614-2230 [71]). Lower asymptotic frequencies down to about 500 Hz are produced by high-mass black holes formed in CC-SNe or mergers of neutron stars with a high-mass black hole companion. Mergers and CC-SNe, hereby, represent distinct astronomical progenitors of long GWBs (and of long GRBs) with a diversity in asymptotic frequencies (2) corresponding to a range in the black hole mass.

The full template follows by integration of the equations of conservation of energy and angular momentum in the process of black hole spin down mostly against the inner face of a surrounding torus [14]

$$\dot{M} = -\kappa(\Omega_H - \Omega_T)\Omega_T, \qquad \dot{J} = -\kappa(\Omega_H - \Omega_T), \quad (3)$$

where $\kappa$ represents the spin connection due to the (variance) in poloidal magnetic field for a black hole in its lowest-energy state, and the angular velocity $\Omega_T$ of the torus is tightly correlated to that at the innermost stable circular orbit (ISCO). As nonaxisymmetries develop [14], $\dot{M}$ and $\dot{J}$ will be carried off mostly in gravitational waves, until the fixed point $\Omega_H = \Omega_T$ is reached at low $a/M$.

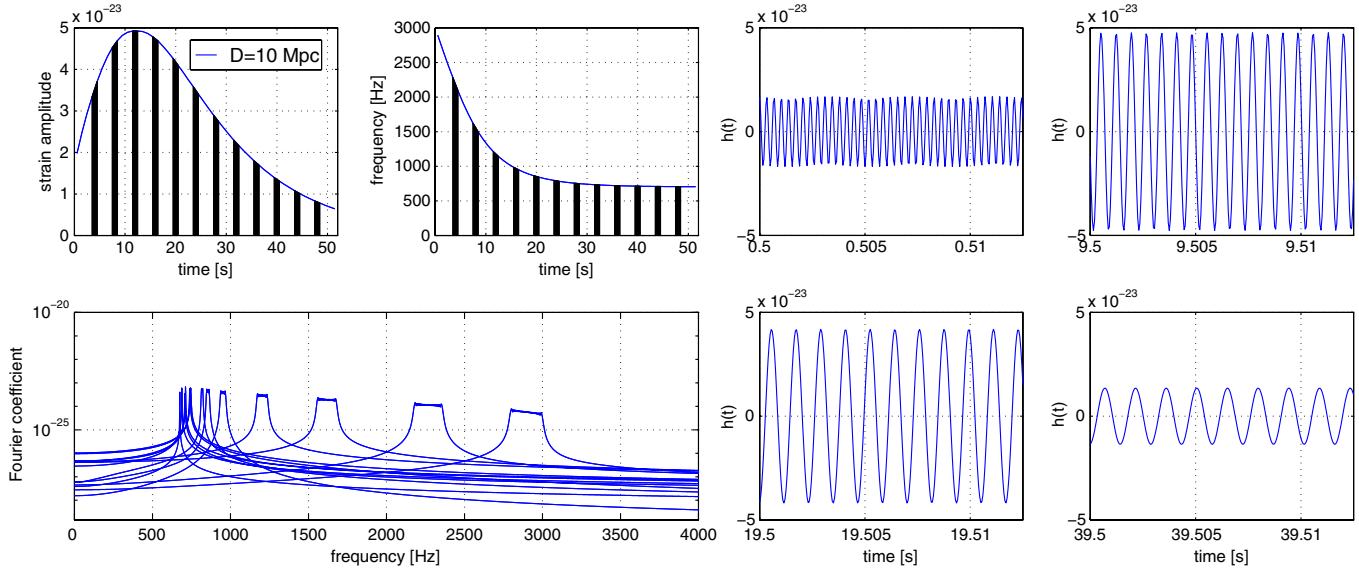


FIG. 1 (color online). (*Left.*) Shown is the evolution of the orientation-averaged strain amplitude of the model template of a long GWB produced by a Kerr black hole of mass $10M_\odot$ at a fiducial distance of 10 Mpc (*left top*) and the negative chirp with a decay in frequency (*right top*) to (2) and associated expansion of the ISCO up to the fixed point $\Omega_H = \Omega_T$ of (3). For time-sliced matched filtering, the template is portioned into segments of intermediate duration, here subwindows of 1 s duration, of which a few are highlighted by the solid bars. Each segment has an effectively band-limited frequency spectrum, shown here for some of the 52 segments (*bottom*). The maximum luminosity is reached when $a/M \simeq 0.8$. For $a/M > 0.8$, the luminosity is less than maximal as $\Omega_T \simeq \Omega_{\rm ISCO}$ remains close to $\Omega_H$. For $a/M < 0.8$, the luminosity decays, as the black hole continues to relax to a slowly spinning, nearly Schwarzschild black hole corresponding to the fixed point $\Omega_H = \Omega_T$. (*Right.*) Snapshots of the model templates for $h_n(t)$ in segments 1, 10, 20, and 40 out of a total of 52.

The resulting gravitational-wave templates are obtained by integration of (3) as a system of two coupled ordinary differential equations in response to an initial mass and spin rate. In [14], we calculated the model templates for different initial values of $a/M$. The resulting strain amplitude and frequency, as seen at Earth for a source at a fiducial distance $D = 10$ Mpc produced by a black hole with initially maximal spin ($a = M$), is shown in Fig. 1. Here, we show the orientation-averaged strain amplitude, which is a factor of $1/\sqrt{5}$ smaller than the amplitude at optimal orientation of the source along the line of sight [72].

In general, the total energy output scales with $M$, and the frequency scales with $M^{-1}$. The strain amplitude scales with $\kappa$ as a function of the mass of the torus relative to $M$ (typically about 0.1–1%), while the total duration of the burst scales with $M$ and $\kappa^{-1}$.

## IV. TIME-SLICED MATCHED FILTERING

The application of matched filtering depends crucially on phase coherence in the true signal, in correlating it to a model template. For a magnetohydrodynamical system powered by a Kerr black hole, turbulence in the inner disk or torus inevitably creates phase incoherence on long time scales, inhibiting the application of matched filtering by correlating to a complete wave-form template with the detector output. To circumvent this limitation, we first slice a model template into $N = T_{90}/\tau$ segments on intermediate time scales, $\tau$, for which phase coherence may be sustained. Matched filtering is now applied using each slice, by correlating each template slice $i$ with the detector output, with the arbitrary offset $\delta$ in time.

We here report on a test of our algorithm on the strain noise amplitude data of the TAMA 300 m detector [73]. TAMA 300 m was the first laser interferometric gravitational-wave detector with long-duration continous operation at a reasonable sensitivity of better than $10^{-20}$ Hz$^{-1/2}$ in strain amplitude noise. Here, we use data from runs DT8 (2/2003–4/2003) and DT9 (11/2003–1/2004) (partially coincident with the LIGO S3 run). The data are sampled at 20 kHz and organized in frames of $2^{20}$ samples (about 52 s). During DT8–9, we note that some 51 CC-SNe have been observed in the local Universe with a mean redshift of 0.024 ($D = 100$ Mpc). Figure 2 shows the detector strain noise amplitude for DT9. Relevant to our exploration of the detector sensitivity to the long GWBs is the high-frequency range between a few hundred and a few thousand Hz. Given this focus and a noticeable increase in the detector strain noise amplitude below 550 Hz, we apply a band filter between 650 and 4000 Hz to the detector strain noise amplitude, where the noise is Gaussian to high precision as shown in Fig. 2. To excellent approximation, therefore, the detector output $h_n(t)$ is represented by the

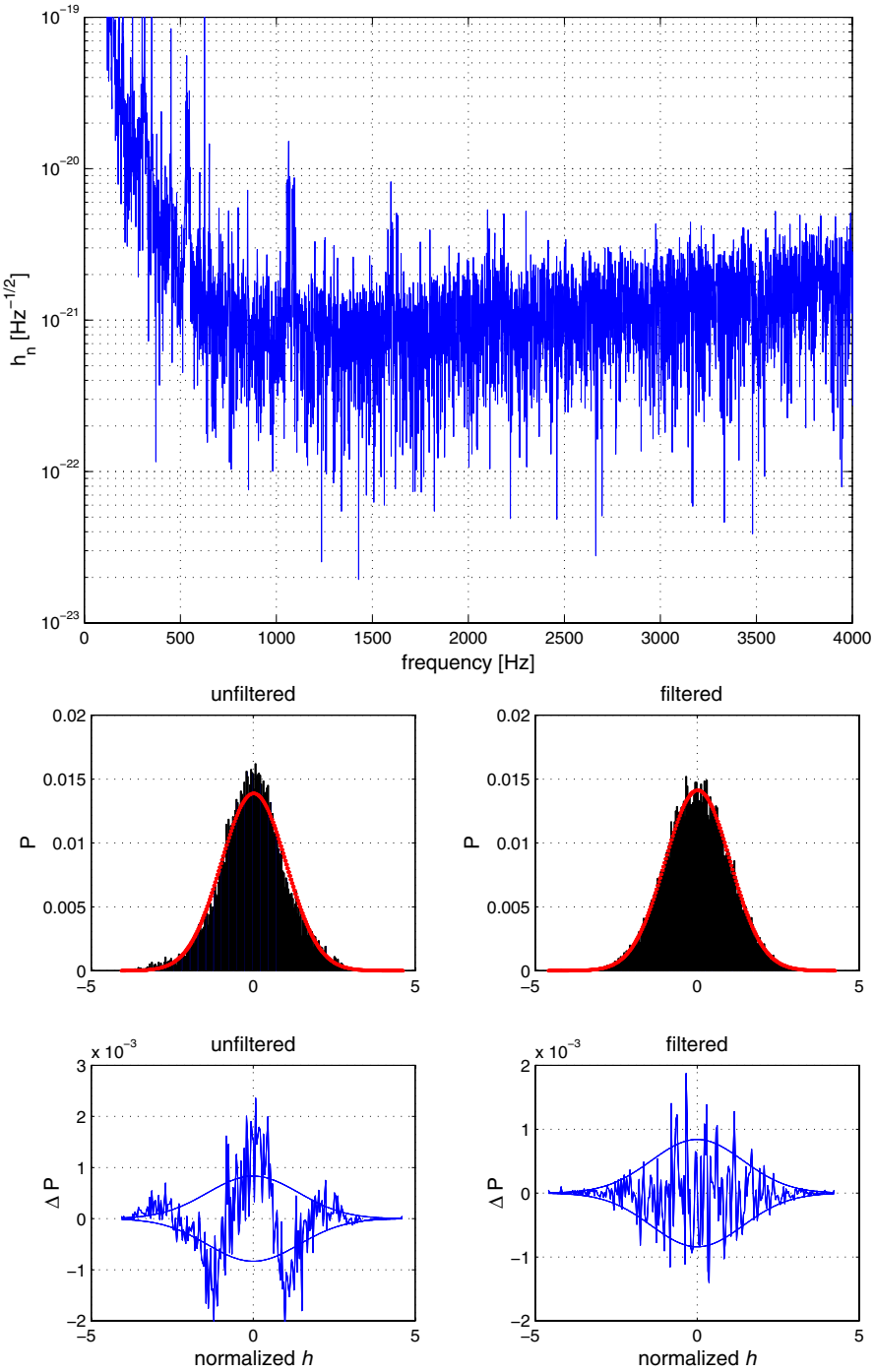


FIG. 2 (color online). (*Top*.) Shown is the TAMA 300 strain noise amplitude in the one-sided frequency domain in the DT9 run of 2003–4 produced by 1 frame of 52 s duration. (*Middle*.) The distribution is non-Gaussian, largely due to low-frequency noise below a few hundred Hz. (*Bottom*.) The fluctuations of the observed probability distribution of the strain noise amplitude over 1 s, normalized to $\sigma = 1$ and plotted over 250 bins of normalized strain noise amplitude $h_n$, about to the Gaussian distribution where $\sigma = 1$ can be compared with the expected fluctuations on the basis of the standard error in the mean in each bin (Standard Error in the Mean, smooth $1 - \sigma$ curves). A band-pass filter across 650–4000 Hz recovers essentially Gaussian noise.

sum of a signal $s(t)$ at the detector and a white additive noise $w(t)$,

$$h(t) = s(t) + w(t), \qquad s(t) = \left(\frac{10\ \mathrm{Mpc}}{D}\right) S(t), \quad (4)$$

where $D$ denotes the source distance and $S(t)$ denotes the template $S(t)$ $(0 < t < T_{90})$ of the signal for a source at a reference distance of 10 Mpc.

For illustrative purposes, we consider a TSMF with intervals $\tau = 1$ s and a burst duration $T_{90}$ of 50 s. Slicing

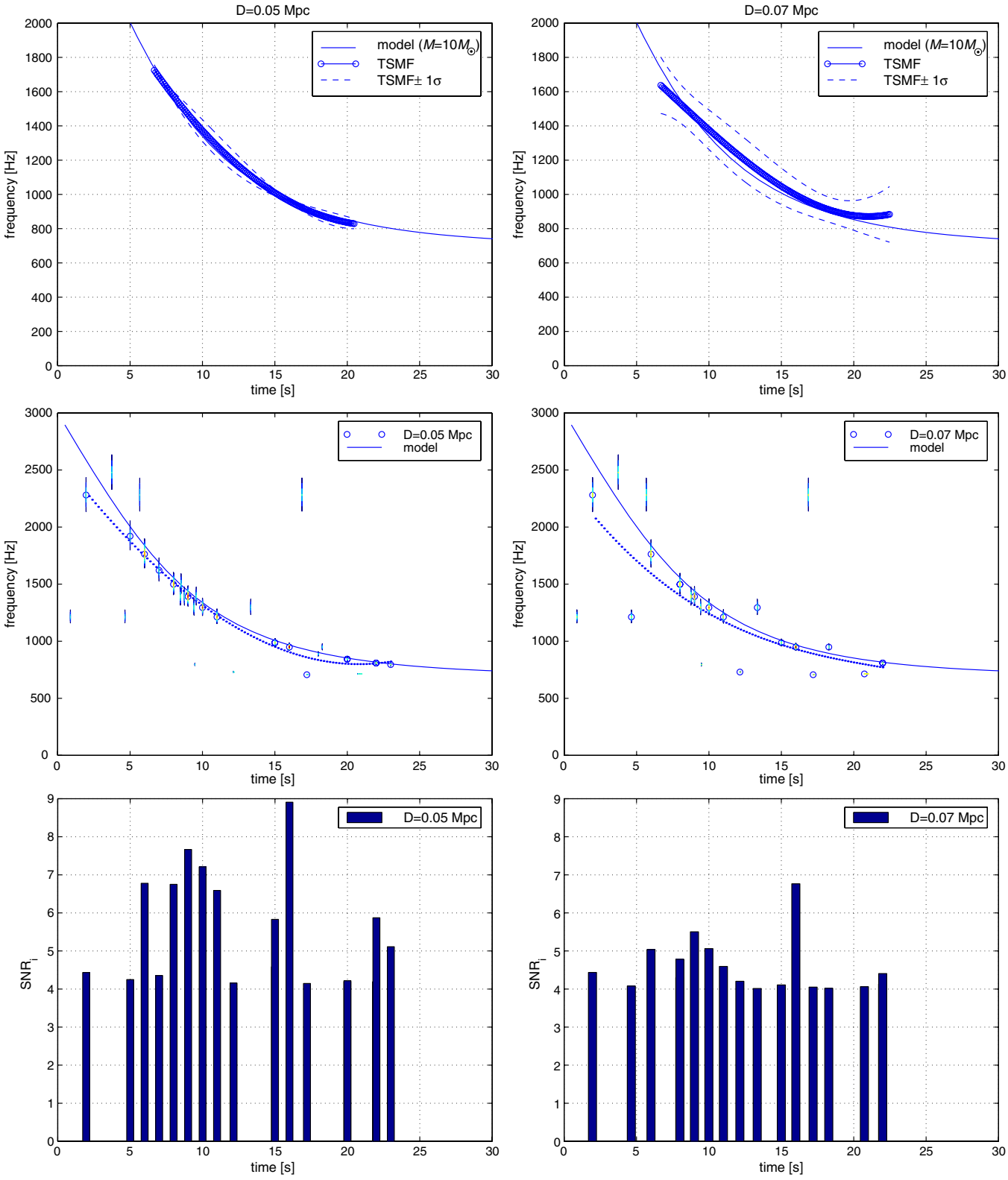


FIG. 3 (color online). (*Top*.) Time-frequency trajectories in the time-frequency domain extracted by TSMF for the spin down of a $M = 10M_\odot$ black hole to a remnant of $8.4M_\odot$. The results shown in the top windows represent the outcome of injections into 10 TAMA 300 frames of 52 s durations for two source distances. (*Middle*.) The extraction is based on the largest SNR $> 4$ in $\rho_i(\delta)$ (on $0 < \delta < 23$ s, containing most of the signal) and, at most, one data point in each of the $\tau = 1$ s bins $i = 1, \ldots, 51$ (*vertical lines*), followed by a polynomial interpolation (*dotted curved line*) of points with reduced scatter (*circles*). (*Bottom*.) The signal-to-noise ratios of the data points used in the polynomial fit.

the template $S(t)$ $(0 < t < T_{90})$ into segments of duration $\tau$ gives $N_s = T_{90}/\tau = 50$ templates $S_i(t)$ for each slice $i$,

$$S_i(t) = S(t_i^* + t), \qquad t_i^* = i\tau, \qquad (i = 1, 2, \ldots, N_s, 0 < t < \tau). \tag{5}$$

Here, it is understood that the time $t$ is discrete, i.e., $t = t_j$, $t_j = (j/N_f)$ s, where $N_f = 20\,000$ denotes the 20 kHz sampling rate of the TAMA 300 detector. TSMF over segments of all data points ($N = N_s \times N_f \simeq 10^6$) in the TAMA 300 data frames starts with computing the Pearson coefficients

$$\rho_i(\delta) = \frac{(S_i \cdot h)_\delta}{||S_i||||h_\delta||} \tag{6}$$

as a function of the unknown offset $\delta = i/20\,000$ $(i = 0, 1, \ldots, N)$ over a complete frame of $N$ samples obtained at the sampling rate of 20 kHz, representing the uncertainty in the continuation of phase between the time slices, where

$$(S_i \cdot h)_\delta = \Sigma_{0<t_j<\tau} S_i(t_i^* + t_j) h(\delta + t_j) \tag{7}$$

denotes the discrete inner product of the $S_i(t_i^* + t_j)$ and the $h(\delta + t_j)$, with $L_2$ norms

$$\begin{aligned} ||S_i|| &= [\Sigma_{0<t_j<\tau} S^2(t_i^* + t_j)]^{1/2}, \\ ||h_\delta|| &= [\Sigma_{0<t_j<\tau} h^2(\delta + t_j)]^{1/2}. \end{aligned} \tag{8}$$

Thus, $\rho_i(\delta)$ represents the cosine between the $S_i$ and $h$ in (6).

To define a signal-to-noise ratio $\mathrm{SNR}_i$ for each slice $i$, we proceed with the normalized Pearson coefficients

$$\hat{\rho}_i(\delta) = \frac{\rho_i(\delta)}{\sigma_i}, \tag{9}$$

where $\sigma_i$ denotes the standard deviation of $\rho_i(\delta)$ as a function of $\delta$, and define

$$\mathrm{SNR}_i = \max_\delta \hat{\rho}_i(\delta). \tag{10}$$

In order to extract a trajectory in the time-frequency domain, we proceed with correlations $\hat{\rho}_i(\delta) > 4$ and select the largest correlation in each time slice. This filter extracts, at most, 52 data points from each frame of 52 s when $\tau = 1$.

Figure 3 shows the statistical results over 10 frames for the spin down of a black hole of $M = 10M_\odot$ at distances of $D = 0.050$ Mpc and $D = 0.070$ Mpc. Here, the extraction of a time-frequency trajectory is performed by polynomial interpolation of the aforementioned $\leq 52$ filtered points with rejection of points with large scatter. Figure 4 indicates a sensitivity distance of about $D \simeq 0.07$–$0.1$ Mpc in the black hole mass range $M = 10$–$12M_\odot$.

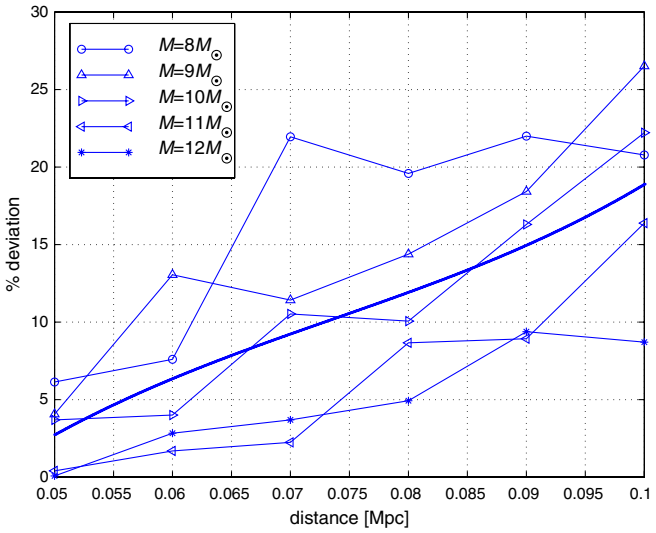


FIG. 4 (color online). Shown is the resulting deviation of the extracted time-frequency trajectory from the model trajectory of the injected signal as a function of distance $D = 0.05$–$0.1$ Mpc and black hole masses $M = 8$–$12M_\odot$. The curved lines represent the standard deviation of the deviations in the extracted trajectories over a common time interval of 12–16 s. The results show sensitivity distances from $D = 0.05$ Mpc for $M = 8M_\odot$ to about $D = 0.1$ Mpc for $M = 12M_\odot$ and the average trend line (*thick line*).

## V. CONCLUSIONS AND OUTLOOK

The diversity in multiwavelength phenomenology on long GRBs strongly suggests a common inner engine that is intrinsically long-lived, representing the outcome of various astronomical scenarios. We here identify the inner engine with rapidly rotating Kerr black holes, whose lifetime is set by the secular time scale of spin in a process of spin down against surrounding high-density matter. At present, the most quantitative observational evidence for black hole spin down is found by matched filtering analysis of 600 light curves of long GRBs in the BATSE catalog [16]. This mechanism points to major contemporaneous emissions in gravitational waves and MeV-neutron emissions that are likely to be dominant over the presently observed electromagnetic radiation in GRB-afterglow emissions and kinetic energies in GRB-SNe. True calorimetry on the inner engine requires observations in these nonelectromagnetic windows.

Most GRBs remain unobserved, due to beaming factors of "a few" to about 500 [33,34]. For CC-SNe, there is a considerable uncertainty of up to several days for the time of onset based on extrapolating backwards in time the supernova optical light curve. Not all long GRBs appear to be associated with CC-SNe, i.e., GRB060614 [48–51] appeared without a bright supernova. If GRB060614 was not an anomalously faint ("failed") supernova, it may have been a merger event [14,15]. Similar considerations apply to the halo event GRB070125, which appeared with no

TABLE II. Estimated $1-\sigma$ uncertainty in the extracted time-frequency trajectories by TSMF as a function of distance applied to long bursts in GWs produced by black hole spin down against high-density matter, expected to form in some of the CC-SNe and mergers of neutron stars with a rapidly rotating companion black hole. We do not include results on neutron-star–neutron-star mergers, in view of their relatively high frequencies of 1.5–2 kHz away from the region of maximal sensitivity of the existing gravitational-wave detectors.

| Mass ($M_\odot$) | $D$[TAMA][a] (Mpc) | $D$[Adv][b] (Mpc) | $R_D$[c] | $\sigma$ | max(SNR$_i$)[d] | sum(SNR$_i$)[e] |
|---|---|---|---|---|---|---|
| 8 | 0.05 | 25 | 0.1 | 6% | 6.4 | 74 |
| 8 | 0.07 | 35 | 0.3 | 22% | 5.0 | 54 |
| 8 | 0.10 | 50 | 1.2 | 27% | 4.5 | 46 |
| 10 | 0.05 | 25 | 0.1 | 4% | 8.2 | 96 |
| 10 | 0.07 | 35 | 0.3 | 11% | 6.2 | 68 |
| 10 | 0.10 | 50 | 1.2 | 22% | 4.9 | 43 |
| 12 | 0.05 | 25 | 0.1 | <1% | 10.5 | 130 |
| 12 | 0.07 | 35 | 0.3 | 4% | 7.8 | 87 |
| 12 | 0.10 | 50 | 1.2 | 9% | 6.0 | 61 |

[a]With $h_n \simeq 10^{-21}$ Hz$^{-1/2}$ at 1 kHz during DT8 (2/2003–4/2003).
[b]With $h_n = 2\times 10^{-24}$ Hz$^{-1/2}$ at 1 kHz.
[c]Estimated event rate within distance $D$[Adv], assuming 10 times more relativistic CC-SNe than successful GRB-SNe with otherwise similar inner engines and the observed event rate of 1 long GRB per year within $D = 100$ Mpc.
[d]Based on $\rho_i(\delta)$, $0 < \delta < 23$ s, $\tau = 1$ s, and averages over 10 frames.
[e]Based on SNR$_i > 4$ and averages over 10 frames.

optically identified host galaxy [52,53]. A significant fraction of binaries exists in globular clusters, as indicated by their population of luminous x-ray sources ([74] and references therein). As the number of globular clusters correlates with the luminosity of elliptical galaxies [75,76], the latter, in particular, may be preferred sites for GRB070125-type events. Therefore, blind, untriggered searches appear to be preferred in searches for local events, exploiting the all-sky survey capability of gravitational-wave detectors.

To explore the sensitivity distance of advanced gravitational-wave detectors to the anticipated long-duration negative chirps from events in the local Universe, we introduce a time-sliced matched filtering algorithm and apply it to the strain noise amplitude of the TAMA 300 detector with signal injection. A time-sliced approach can circumvent the limitations posed by phase incoherence on the time scale of the duration of the burst, which generally inhibits optimal matched filtering using complete wave-form templates. By injecting our model template into the strain noise data of the TAMA 300 detector during a run with $h_n(t) \simeq 1\times 10^{-21}$ Hz$^{-1/2}$, we compute correlations between the $i$-th time slice (of duration $\tau$) and one frame (about 52 s) of detector output.

For a typical black hole mass of $10M_\odot$, the results indicate the importance of the middle- and late-time behavior of the bursts (Fig. 3) below 2000 Hz, but less so the initial spin-down phase associated with higher frequencies when starting from a maximal rotation. This reduction results from the relatively large strain amplitude noise of the detector in the shot-noise region for frequencies of a few kHz. Effectively, the search is focused on the output post-maximum ($a/M < 0.8$), which obviates the need to consider templates over a wide range of initial spin. A complete search will include a scan over two parameters: a range of intermediate time scales, e.g., $\tau = 0.1$–1, and scaling of frequencies of the templates to account for a diversity in black hole masses, e.g., between $5$–$15M_\odot$. The range $\tau = 0.1$–1 s represents tens to hundreds of orbital periods of the torus. This time scale in the coherent evolution of the torus might correspond to those of sub-bursts in the light curves of long GRBs (e.g., [4]), and the quasisteady evolution of the torus on a time scale of at least tens of orbital periods follows from an upper bound of about 10% on the electromagnetic field energy it can support, relative to its kinetic energy [20].

Our estimated TAMA 300 sensitivity distance for extracting time-frequency trajectories is summarized in Table II. The results show $D \simeq 0.070$–$0.10$ Mpc for black holes in the mass range $M = 10$–$12M_\odot$, which compares favorably with the sensitivity distance for neutron-star–neutron-star coalescence. Extrapolation points to a sensitivity distance $D \simeq 35$–$50$ Mpc for a strain noise amplitude of $2\times 10^{-24}$ Hz$^{-1/2}$ in the planned advanced detectors LIGO-Virgo and the Large-scale Cryogenic Gravitational-wave Telescope. This sensitivity distance serves as a conservative estimate for the sensitivity distance for a detection. In particular, the sums of the 15 SNR$_i$'s shown in Fig. 4 are 95 and 77 for $D = 0.05$ Mpc and $D = 0.07$ Mpc, respectively. These sums point to a sensitivity distance for a detection (with no particular information of behavior in the time-frequency domain)

on the order of a few tenths of Mpc, corresponding to a sensitivity distance of well over 100 Mpc for the advanced detectors.

Based on the observed event rate of long GRBs of about 1 per year within a distance of 100 Mpc, the observable event rate suitable for extracting time-frequency trajectories will depend on the abundance of the parent population of aspherical, relativistic and radio-loud type Ib/c SNe that may be powered by the irradiation of the stellar envelope from a long-lived black hole inner engine [77]. It may reach one per every few years if their event rate is about 1 order of magnitude larger than the rate of successful GRB supernovae. The observable event rate could be larger if a fraction of the supernovae of type II is similarly powered by long-lived black hole inner engines. A much larger sensitivity distance is anticipated for the planned 10 km Einstein Telescope in Europe. Conceivably, all-sky radio surveys, e.g., the LOw Frequency ARray [78], will further provide us with a probe for long-duration radio bursts from mergers [13] and, combined with gravitational-wave surveys, provide a direct measurement of the relative event rates of long GRBs from mergers to long GRBs from CC-SNe.

The diversity in the origin of long GRBs in both CC-SNe and mergers [13] and the comparable sensitivity distances of their potential emissions in gravitational waves and those from binary coalescence suggests the need for extended searches over the complete frequency ranges of both. Apart from scaling by black hole mass and a diversity in initial spin, the proposed long GWBs are universal, and their progenitors are revealed only by the absence or presence of a precursor signal in gravitational waves in the case of, respectively, a CC-SNe or merger event.

## ACKNOWLEDGMENTS

The initial work for this research was partially supported by La Région Centre during a visit to Le STUDIUM Institute for Advanced Studies/CNRS-Orléans. The authors gratefully acknowledge the TAMA Collaboration for providing the data. M. V. P. thanks Lars Hernquist and Ramesh Narayan for stimulating discussions.

[1] M. H. P. M. van Putten and A. Levinson, Science **295**, 1874 (2002).
[2] S. Woosley, Astrophys. J. **405**, 273 (1993).
[3] B. P. Paczyński, Acta Astronaut. **41**, 257 (1991).
[4] M. H. P. M. van Putten, Science **284**, 115 (1999).
[5] M. H. P. M. van Putten and E. C. Ostriker, Astrophys. J. **552**, L63 (2001).
[6] N. Gehrels *et al.*, Nature (London) **437**, 851 (2005).
[7] J. S. Villasenor, Nature (London) **437**, 855 (2005).
[8] D. B. Fox *et al.*, Nature (London) **437**, 845 (2005).
[9] J. Hjörth *et al.*, Nature (London) **437**, 859 (2005).
[10] B. P. Paczyński, Astrophys. J. **494**, L45 (1998).
[11] M. H. P. M. van Putten, Astrophys. J. **611**, L81 (2004).
[12] L. Baiotti, B. Giacomazzo, and L. Rezzolla, Phys. Rev. D **78**, 084033 (2008).
[13] M. H. P. M. van Putten, Mon. Not. R. Astron. Soc. Lett. **396**, L81 (2009).
[14] M. H. P. M. van Putten, Astrophys. J. **684**, L91 (2008).
[15] L. Caito, M. G. Bernardini, C. L. Bianco, M. G. Dainotti, R. Guida, and R. Ruffini, Astron. Astrophys. **498**, 501 (2009).
[16] M. H. P. M. van Putten and A. C. Gupta, Mon. Not. R. Astron. Soc. **394**, 2238 (2009).
[17] S. B. Cenko *et al.*, Astrophys. J. **711**, 641 (2010).
[18] S. B. Cenko *et al.*, arXiv:1004.2900.
[19] M. H. P. M. van Putten, Phys. Rep. **345**, 1 (2001).
[20] M. H. P. M. van Putten and A. Levinson, Astrophys. J. **584**, 937 (2003).
[21] B. Barish and R. Weiss, Phys. Today **52**, 44 (1999).
[22] F. Arcese *et al.*, Classical Quantum Gravity **21**, S385 (2004).
[23] K. Kuroda *et al.* (LCGT Collaboration), Classical Quantum Gravity **27**, 084004 (2010).
[24] S. Hild, S. Chelkowski, and A. Friese, arXiv:0810.0604.
[25] D. Guetta and M. Della Valle, Astrophys. J. **657**, L73 (2007).
[26] R. O'Shaughnessy *et al.*, Astrophys. J. **672**, 479 (2008).
[27] J. Abadie *et al.*, Classical Quantum Gravity **27**, 173001 (2010).
[28] M. Della Valle, Mem. Soc. Astron. Ital. **81**, 367 (2010).
[29] E. Cappellaro, R. Evans, and M. Turatto, Astron. Astrophys. **351**, 459 (1999).
[30] F. Mannucci, M. Della Valle, and N. Panagia *et al.*, Astron. Astrophys. **433**, 807 (2005).
[31] P. Höflich, J. C. Wheeler, and L. Wang, Astrophys. J. **521**, 179 (1999).
[32] S. Ishikawa, S. Yamada, M. Kiguchi, and K. Sato, Astron. Astrophys. **258**, 415 (1992).
[33] D. A. Frail *et al.*, Astrophys. J. **562**, L55 (2001).
[34] M. H. P. M. van Putten and T. Regimbau, Astrophys. J. **593**, L15 (2003).
[35] R. Sari, Astrophys. J. **494**, L49 (1998).
[36] R. Chevalier and Z.-Y. Li, Astrophys. J. **536**, 195 (2000).
[37] D. Band *et al.*, GRB Coordinates Network, Circular Service, 3734 (2005).
[38] J. U. Fynbo *et al.*, GRB Coordinates Network, Circular Service, 3749 (2005); 3756 (2005).
[39] G. Cusumano *et al.*, Astron. Astrophys. **462**, 73 (2007).
[40] T. Sakamoto, L. Barbier, and S. Barthelmy *et al.*, GRB Coordinates Network, Circular Service, 3938 (2005).
[41] E. Berger *et al.*, Astrophys. J. **660**, 496 (2007).
[42] E. Berger *et al.*, Astrophys. J. **665**, 102 (2007).

[43] A. D. Falcone *et al.*, GRB Coordinates Network, Circular Service, 4966 (2006).
[44] J. X. Prochaska *et al.*, Astrophys. J. Suppl. Ser. **168**, 231 (2007).
[45] J. Cummings, L. Barbier, S. Barthelmy *et al.*, GRB Coordinates Network, Circular Service, 4975 (2006).
[46] S. Covino *et al.*, Chin. J. Astron. Astrophys. **8**, 356 (2008).
[47] P. Jakobsson and J. P. U. Fynbo, arXhiv:0704.1421.
[48] M. Della Valle *et al.*, Nature (London) **444**, 1050 (2006).
[49] J. P. U. Fynbo *et al.*, Nature (London) **444**, 1047 (2006).
[50] N. Gerhels *et al.*, Nature (London) **444**, 1044 (2006).
[51] A. Gal-Yam *et al.*, Astrophys. J. **639**, 331 (2006); Nature (London) **444**, 1053 (2006).
[52] S. B. Cenko *et al.*, Astrophys. J. **677**, 441 (2008).
[53] P. Chandra *et al.*, Astrophys. J. **683**, 924 (2008).
[54] J. L. Racusin, S. V. Karpov, M. Sokolowski *et al.*, Nature (London) **455**, 183 (2008).
[55] N. R. Tanvir, E. Rol, A. J. Levan *et al.*, Astrophys. J. **725**, 625 (2010).
[56] J. S. Bloom *et al.*, Astrophys. J. **691**, 723 (2009).
[57] D. A. Frail *et al.*, Astrophys. J. **646**, L99 (2006).
[58] K. L. Page *et al.*, Astrophys. J. **637**, L13 (2006).
[59] H. Pedersen *et al.*, Astrophys. J. **496**, 311 (1998).
[60] D. A. Frail *et al.*, Astrophys. J. **538**, L129 (2000).
[61] P. Kumar and T. Piran, Astrophys. J. **535**, 152 (2000).
[62] E. Ramirez-Ruiz, A. Celotti, and M. J. Rees, Mon. Not. R. Astron. Soc. **337**, 1349 (2002).
[63] E. Berger *et al.*, Nature (London) **426**, 154 (2003).
[64] Y. F. Huang *et al.*, Astrophys. J. **605** 300 (2004).
[65] F. Peng, A. Königl, and J. Granot, Astrophys. J. **626**, 966 (2005).
[66] B. Carter, Phys. Rev. **174** 1559 (1968).
[67] R. M. Wald, Phys. Rev. D **10**, 1680 (1974).
[68] R. Ruffini and J. R. Wilson, Phys. Rev. D **12**, 2959 (1975).
[69] V. I. Dokuchaev, Sov. Phys. JETP **65**, 1079 (1987).
[70] D. Nice, E. M. Splaver, and I. H. Stairs *et al.*, Astrophys. J. **634**, 1242 (2005).
[71] P. B. Demorest, T. Pennucci, S. M. Ransom, M. S. E. Roberts, and J. W. T. Hessels, Nature (London) **467**, 1081 (2010).
[72] E. Flanagan and S. A. Hughes, Phys. Rev. D **57**, 4535 (1998).
[73] R. Takahashi *et al.*, Classical Quantum Gravity **21**, S403 (2004).
[74] F. Verbunt and W. H. G. Lewin, in *Compact Stellar X-ray Sources*, edited by W. H. G. Lewin and Michiel van der Klis (Cambridge University Press, Cambridge, England, 2005), Chap. 8.
[75] W. E. Harris and S. van den Bergh, Astron. J. **86**, 1627 (1981).
[76] A. Burkert and S. Tremaine, Astrophys. J. **720**, 516 (2010).
[77] M. H. P. M. van Putten, Astrophys. J. **583**, 374 (2003).
[78] LOFAR, 2010, http://lofar.org.